



# Increase of gas–liquid interfacial area in bubbly flows by pulsating flow conditions

Sotiris P. Evgenidis<sup>\*</sup>, Thodoris D. Karapantsios

Department of Chemical Technology and Industrial Chemistry, School of Chemistry, Aristotle University, University Box 116, 541 24 Thessaloniki, Greece

## ARTICLE INFO

### Keywords:

Void fraction  
Bubble size  
Decompression Sickness  
Pulsating flow  
Two-phase flow  
Electrical impedance

## ABSTRACT

This work investigates for the first time in-vitro the pulsating gas–liquid flow of sub-mm bubbles at low void fractions ( $<10^{-1}$ ) that resembles bubbly flow in human vena cava during Decompression Sickness and can be also found in reactors utilized for the treatment of municipal sewage. Void fraction and Bubble Size Distribution are experimentally studied by means of electrical impedance spectroscopy and image processing, respectively. Experiments are conducted in water and blood simulant, while bubble size varies using prescribed surfactant concentrations. The influence of gas superficial velocity, surfactant concentration, liquid properties and pulsating flow parameters (pulse type and duty cycle, single-phase/liquid vs two-phase/gas–liquid pulsating flow) is discussed in details. Interestingly, pulsating conditions disintegrate bubbles of a few hundreds  $\mu\text{m}$  into smaller ones, while void fraction increases inversely with pulse duty cycle. Consequently, proper tuning of pulsation may enhance gas–liquid mass transfer in industrial applications due to induced gas–liquid interfacial area increase. Periodic void fraction fluctuation features depend strongly on the type (square or sinusoidal) and duty cycle of applied pulse, but practically do not differ between single-phase and two-phase pulsating conditions when employing comparable pulsations.

## 1. Introduction

In physiological and technological systems, transport of mass and energy through fluid flow is usually unsteady. In fluid mechanic studies, the introduction of flow unsteadiness results in complex fluid dynamic behavior and, additionally, requires measurement diagnostics of high temporal resolution. In-depth understanding of time-dependent and particularly time-periodic (pulsating) flow dynamics, however, contributes to the optimization of several processes through the exploitation of unsteady mass, momentum and energy transfer [1,2].

Pulsating flows are characterized by the periodic variation of one or more flow parameters. Single-phase pulsating flows are encountered in several industrial and medical applications. Interestingly, they seem to be usually beneficial to physico-chemical processes. For instance, the performance of catalytic processes can be improved under unsteady flow conditions, while time-periodic flows in pipes may enhance mass transport through permeable walls or removal of deposits during biomaterial processing. Pulsating fluid flows exist also in combustion engines and reciprocating compressor systems [3–5]. In humans, on the other hand, pulsating flow of bodily fluids which plays essential role in

regulating the functions of cells and organs concerns: a) Blood in the circulatory system, b) Air in the respiratory system and c) Cerebrospinal fluid in the brain [6,7].

Two-phase (gas–liquid) pulsating flows are also found both in industry and human physiology. Their utilization in industrial applications is associated to the intensification of different physico-chemical processes. Pulsating slug and annular flow, for example, is encountered in pulsating heat pipes (PHPs). PHPs are two-phase passive cooling devices where the heat transfer rate is higher than that of other conventional heat pipes. They are extensively applied in heat recovery systems, electronic cooling systems, space, automobiles, solar and thermal energy, taking the advantage of their simple structure, fast thermal response, higher heat transfer rate and simple construction [8,9]. Also, pulsating bubbly flow is applied to Conventional Activated Sludge (CAS) systems for the treatment of municipal sewage. CAS are intensified reactors featuring high bacterial loads and relatively short hydraulic residence time. The reactor efficiency depends strongly on the instant supply of dissolved oxygen constantly consumed by the bacteria as they decompose the organics and it has been shown that pulsating bubbly flow conditions increase significantly mass oxygen transfer [10]. In addition, gas–liquid inter-phase mass transfer is further enhanced when

<sup>\*</sup> Corresponding author.

E-mail address: [sevgenid@chem.auth.gr](mailto:sevgenid@chem.auth.gr) (S.P. Evgenidis).

### Nomenclature

$\epsilon$	void fraction
AHS	Active Hydrophobic Spots
BSD	Bubble Size Distribution
CFD	Computational Fluid Dynamics
$C_{SDS}$	concentration of SDS
$D$	internal pipe diameter
$D_{1,0}$	arithmetic mean bubble diameter of a BSD
DCS	Decompression Sickness
PHP	Pulsating Heat Pipe
$Re$	Reynolds number of liquid phase
SDS	Sodium Dodecyl Sulfate
$StDev(D_{1,0})$	Standard deviation around $D_{1,0}$ of a BSD
$U_{sg}$	gas superficial velocity
$U_{sl}$	liquid superficial velocity

reducing bubble size below 1 mm due to gas–liquid interfacial area increase [11]. In human physiology, pulsating bubbly flow can occur when gas bubbles get into the blood stream, either during Decompression Sickness (DCS) incidents, e.g. in astronauts, divers and metro workers, or during cardio-vascular surgeries due to extracorporeal blood circulation circuit malfunction. In DCS, a cloud of growing, sub-millimeter bubbles form directly inside the bloodstream by desorption of dissolved breathing nitrogen in the blood, while in the cardio-vascular surgeries, a few bubbles of fixed size ranging from micrometers to millimeters accidentally enter the blood circulation. Either because of their size or number, bubbles can cause pathologies as a result of mechanical, physiological or biochemical effects. On the contrary to the undesirable formation of bubbles in the human body, however, bubbles can be introduced into the blood stream deliberately to block the blood supply to tumours in blood vessels [1,12].

This study is focused primarily on the pulsating bubbly flow encountered in human physiology, as a result of bubbles formation due to decompression. So far, different researchers have investigated both numerically and experimentally the behavior of decompression bubbles in the body. Nikolayev [13] simulated mathematically the growth and dissolution of gas bubbles which may be formed in the tissues of a diver performing a typical diving with air as the breathing mixture. Also, Zueco and Hernandez-Gonzalez [14] and Zueco and Lopez-Gonzalez [15] studied numerically the dynamics of extravascular bubbles formed in intercellular cavities of a hypothetical tissue undergoing decompression, where emphasis was given to the influence of bubble size, nitrogen tension, nitrogen diffusivity and solubility, ambient pressure and specific blood flow through the tissue.

Bubbles nucleation and expansion after decompression has been investigated ex-vivo in calm conditions, using blood vessels and tissues of different experimental animals. Arieli and Marmur [16,17] and Arieli et al. [18] showed that after decompression of ovine large blood vessels from high pressure, bubbles nucleate and expand at active hydrophobic spots (AHS) on their luminal aspect. AHS were created by surfactant leaks from the lung into the bloodstream and settling on the luminal aspect of blood vessels. Nano-bubbles formed by dissolved gas at these AHS are most probably the precursors of gas micronuclei and decompression bubbles which cause the most severe DCS. Papadopoulou et al. [12] compared bubble growth due to decompression on different tissue surfaces, rabbit muscle and fat, and found that detachment sizes (last size before bubbles float) are significantly different:  $439 \pm 52 \mu\text{m}$  for fat versus  $213 \pm 52 \mu\text{m}$  for muscle. Gas bubble formation during the reduction of ambient pressure has been also studied ex-vivo in rat brain slices by Blatteau et al. [19]. However, none of the above studies investigated the flow of the medium surrounding the bubble. Arieli and Marmur [20] and Arieli [21] conducted for the first time optical

recording of three decompressed sheep blood vessels (aorta, pulmonary artery and pulmonary vein) under pulsating flow of supersaturated saline and showed that bubbles expand from a diameter of 0.1 mm to 1 mm in 2–24 min and detach with a diameter ranging from 0.5 mm to 1.5 mm.

Further research is still needed to improve the understanding around DCS, since a non-negligible percentage of patients suffering from the disease exhibit incomplete recovery despite state-of-the-art hyperbaric oxygen treatment in decompression chambers [19]. Although numerous studies investigate bubbles nucleation and growth on tissue surfaces due to decompression, literature lacks of research on bubbly flow arising from bubbles detachment and entry in the blood flow.

Here, we attempt to fill this gap in the literature conducting in-vitro experimental study of vertical, co-current, upward, pulsating gas–liquid flow, where the examined conditions simulate bubbly flow in human vena cava during DCS. Despite the different local characteristics, similar pulsating gas–liquid flows with sub-millimeter bubbles are also encountered in modern reactors utilized for the treatment of municipal sewage [10]. This work complements our previous studies that investigated in-depth this bubbly flow case for similar conditions, except the type of flow (steady instead of pulsating), using both Newtonian and non-Newtonian blood simulant liquids. Specifically, void fraction,  $\epsilon$ , and bubble size distribution, BSD, were experimentally investigated along and across the vertical pipe in a fully automated flow-loop by means of electrical (impedance spectroscopy -EP 3005942 A1, 2016- and resistance tomography), optical and pressure (absolute and differential) diagnostics [22–25]. Moreover, we examined and optimized different drift-flux model based correlations for the prediction of void fraction in such unusual conditions combining sub-millimeter bubbles and low  $\epsilon$  values ( $<10^{-1}$ ) [26] and performed 2D and 3D CFD (Computational Fluid Dynamics) simulations to study the evolution of void fraction and velocity profiles along the vertical pipe and a realistic human artery as well [27,28]. The present study will extend the abovementioned knowledge by investigating for the first time the effect of liquid properties (viscosity, salinity, surface tension), gas velocity and flow pulsation characteristics (pulse type and duty cycle, single-phase/liquid vs two-phase/gas–liquid pulsating flow) on void fraction and BSD features during pulsating bubbly flow that mimics DCS conditions. Thus, it will contribute in the improvement of the prevention and treatment of the disease as well as in the optimization of industrial processes including pulsating flow conditions.

## 2. Materials and methods

Fig. 1 shows the schematic representation of the experimental setup used to investigate pulsating bubbly flow that imitates DCS conditions. Since its components and operation have been analytically described in our past studies referring to steady flow conditions [22], here we present briefly the experimental setup and focus mostly on the generation of pulsating flow conditions. The measurements are performed in a vertical co-current upward two-phase (gas–liquid) flow provided by a fully controllable flow loop, which can generate steady and pulsating flow at various gas/liquid flow rates and bubble sizes. The vertical tube inside which upward bubbly flow occurs has a length of 1.6 m and an internal diameter ( $D$ ) of 21 mm, which is equal to the diameter of human vena cava where bubbles gather during DCS [29]. It accommodates successive test sections of electrical, optical, acoustical and pressure diagnostics to measure void fraction, bubble size and bubble velocity along it. Test liquid recirculates in the flow loop using a progressive cavity pump (MD 025-6L, Motovario S.p.A.; P-1 in Fig. 1), while micro-bubbles are injected in the flowing liquid through the pores of a cylindrical glass filter (ROBU®, nominal pore size: 1.0–1.6  $\mu\text{m}$ ; GPF-1 in Fig. 1) located at the center of the bottom of the vertical tube. Pulsating flow conditions are applied both in liquid (single-phase) flow and gas–liquid (two-phase) flow to simulate bubbles formation in vessels away from and close to the heart, respectively. To create pulsating liquid flow through the flow-

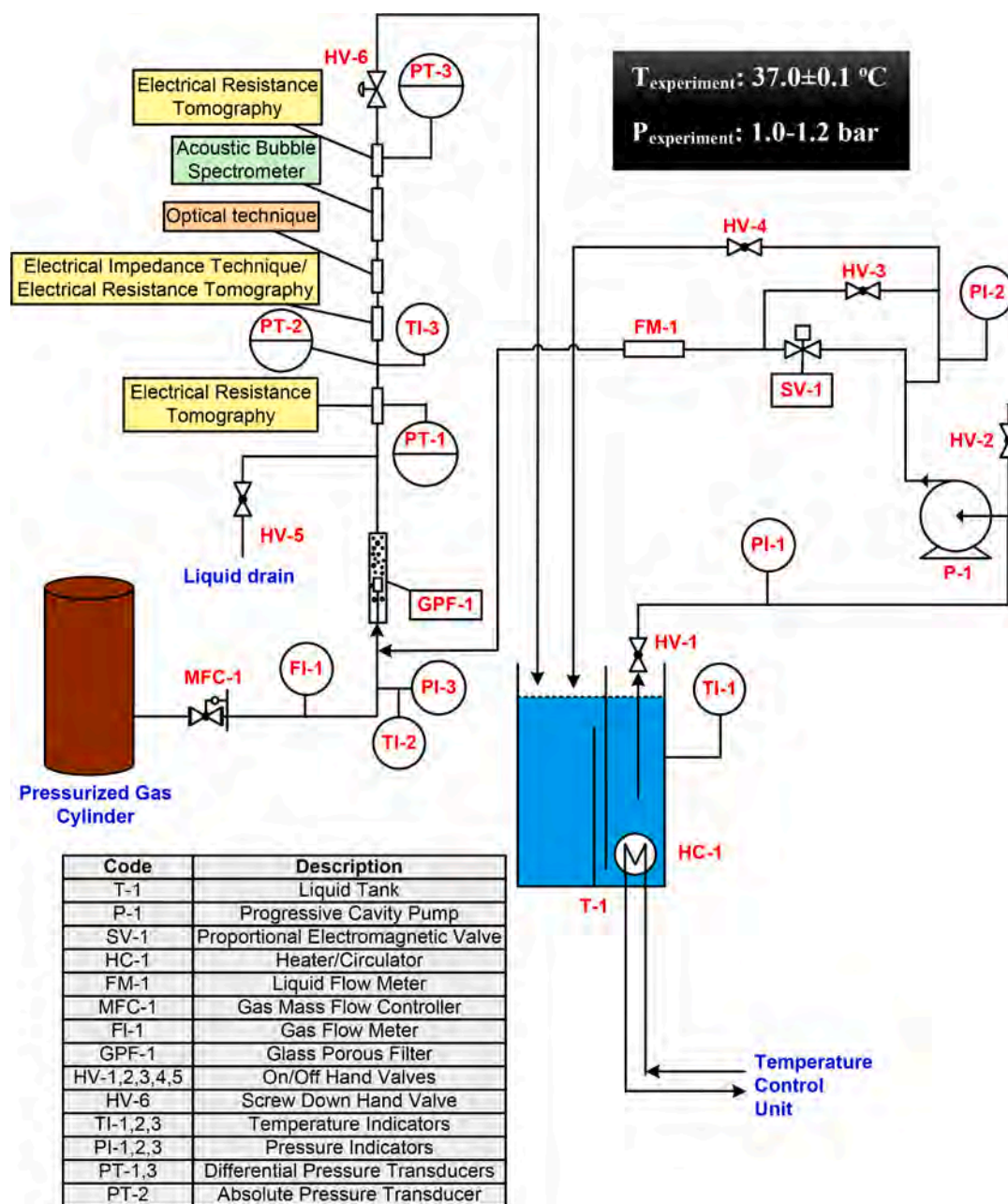


Fig. 1. Schematic representation of the experimental setup.

loop, we employ an intermittent flow module prior to gas injection point that includes:

- A proportional electromagnetic valve placed at the horizontal pipe that precedes the vertical one along the flow (PSV, Alborg, SV-1 in Fig. 1).
- A function generator (20 MHz Function/Arbitrary Waveform Generator, 33220A, Agilent) that produces the electrical signal of varying pulsation frequency, amplitude, profile (sinusoidal, triangular or square) and duty cycle which drives the valve. Duty cycle (%) defines the time percentage of the square pulse duration where the valve is open (e.g. for a pulse frequency of 1 Hz that corresponds to a pulse duration of 1 s, a duty cycle of 80 % indicates that the valve is open for 0.8 s and closed for the remaining 0.2 s). As valve closes periodically based on the employed pulse features, it interrupts periodically single-phase or two-phase flow and results in pulsating flow conditions. When duty cycle comes close to 100 %, pulsating

flow approaches steady flow; on the other hand, decrease of duty cycle increases the intensity of flow pulsation.

- An electronic driver (PSV-D Driver Module, Alborg) that modulates the valve.

In the case of two-phase (gas-liquid) pulsating flow, the proportional electromagnetic valve is moved to the vertical tube, 15 cm (~7D) above the gas injection point. Relative pressure measurements, performed by a piezo-electric transducer (401001, JUMO MIDAS, PT-2 in Fig. 1) at an axial distance of 53 cm (~25D) from the gas injection point and recorded by NI DAQPad-6015, allow monitoring of flow pulsations along the vertical tube.

Void fraction and bubble size constitute the two key quantities under study. Void fraction measurements are performed with an EU patented electrical impedance spectroscopy technique (EP 3005942 A1, 2016) of exceptional spatial and temporal resolution, called *I-VED*. *I-VED* has been originally developed in the framework of a European Space Agency

**Table 1**  
Measured physical properties of test liquids at 37 °C.

Test liquid	Composition	SDS (ppm)	Surface tension (mN/m)	Density (kg/m <sup>3</sup> )	Electrical conductivity (mS/cm)*	Dynamic viscosity (mPa.s)
Water	NaCl (0.02 % w/w)	5	67.0	995	0.5	0.70
	aqueous solution	500	37.0	991	0.5	0.70
Blood	Glycerol (56.0 % w/w) / NaCl (1.3 % w/w)	–	68.0	1149	5.4	4.85
	aqueous solution	500	34.0	1144	5.4	5.10

\* Measured at at 25 °C.

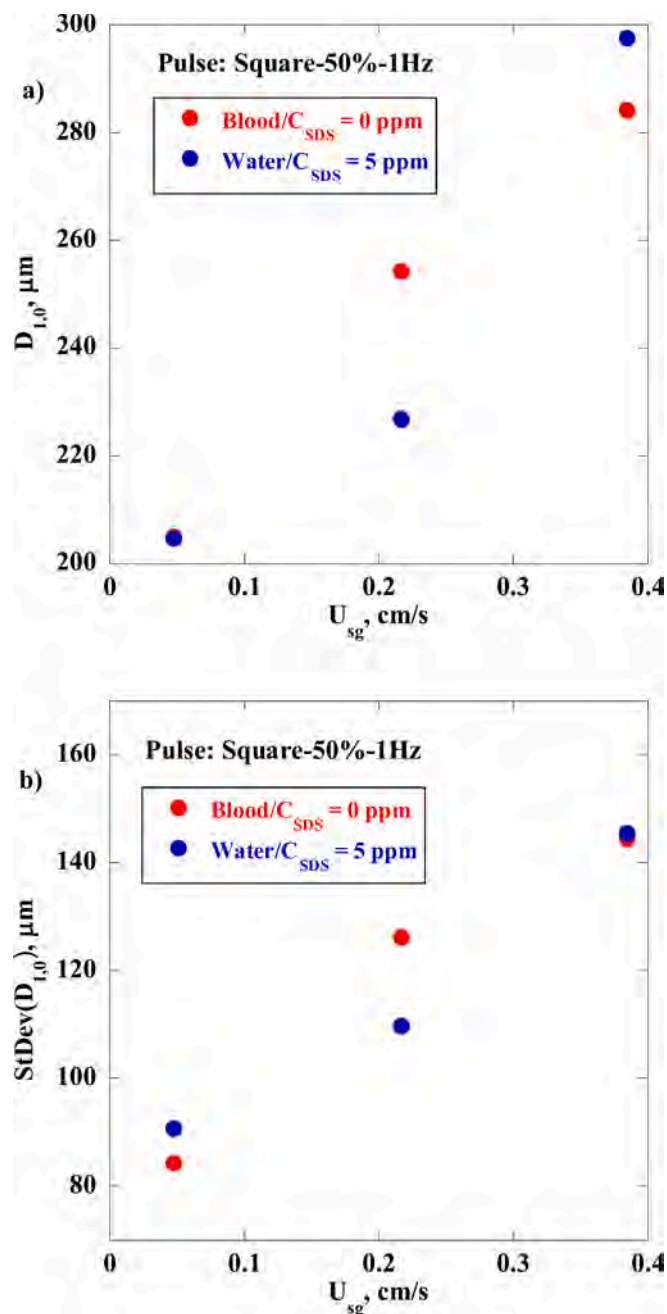


**Fig. 2.** Effect of gas superficial velocity,  $U_{sg}$ , on a) the arithmetic average bubble diameter,  $D_{1,0}$ , and b) the corresponding standard deviation,  $StDev(D_{1,0})$ , of the BSDs in Water with  $C_{SDS} = 5$  ppm and Blood with  $C_{SDS} = 0$  ppm, when applying a square pulse with duty cycle 50 % and frequency 1 Hz to liquid flow (resulting  $U_{sl} = 2.89 \pm 0.96$  cm/s).

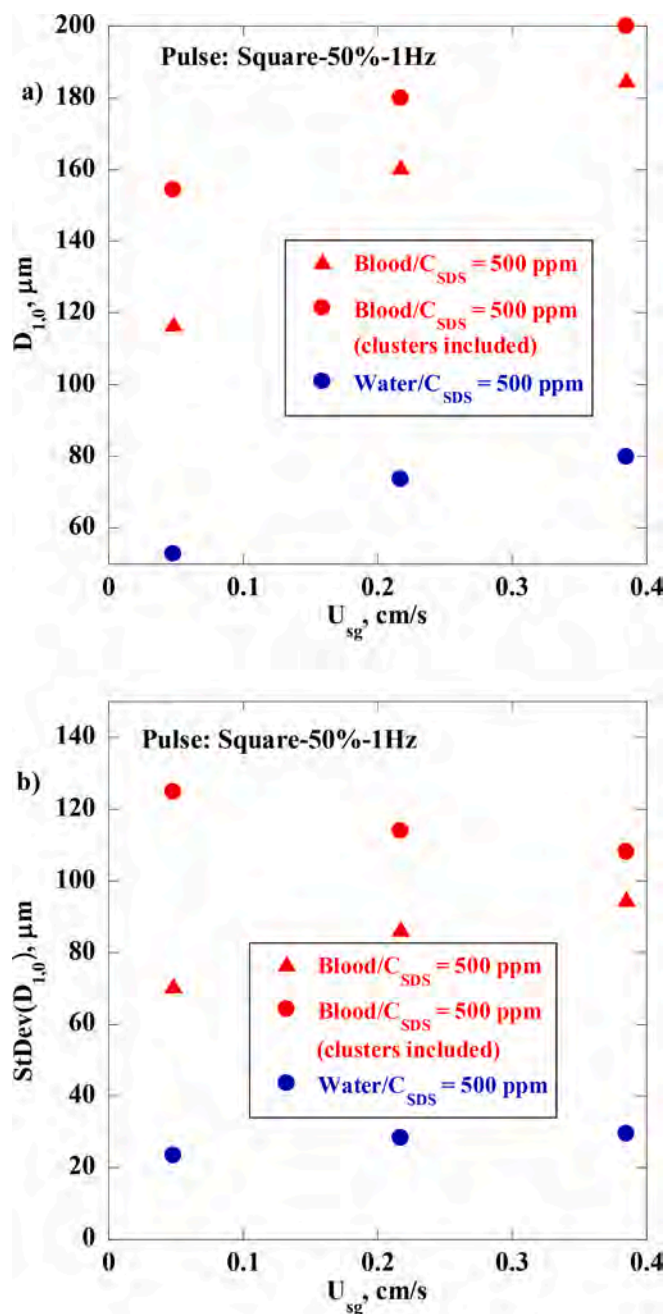


**Fig. 3.** Effect of gas superficial velocity,  $U_{sg}$ , on a) the arithmetic average bubble diameter,  $D_{1,0}$ , and b) the corresponding standard deviation,  $StDev(D_{1,0})$ , of the BSDs in Water and Blood with  $C_{SDS} = 500$  ppm, when applying a square pulse with duty cycle 50 % and frequency 1 Hz to liquid flow (resulting  $U_{sl} = 2.89 \pm 0.96$  cm/s).

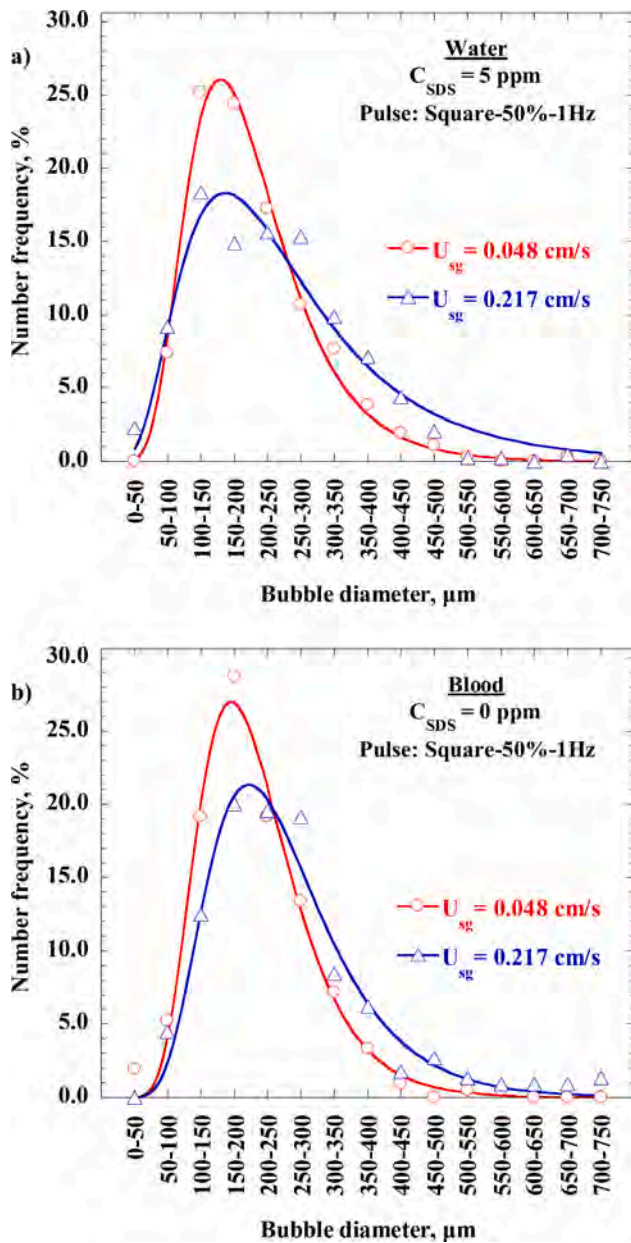


Fig. 4. Bubble Size Distributions for varying gas superficial velocity ( $U_{sg}$ ) in a) Water with  $C_{SDS} = 5$  ppm and b) Blood with  $C_{SDS} = 0$  ppm, when applying a square pulse with duty cycle 50 % and frequency 1 Hz to liquid flow (resulting  $U_{sl} = 2.89 \pm 0.96$  cm/s).

GSTP Project (Contract No.: 4000101764, 2005–2015) for the detection of bubbles in astronauts' bloodstream during Decompression Sickness. It offers 2–3 orders of magnitude higher sensitivity and accuracy compared to other conventional electrical techniques, allowing to capture void fraction fluctuations down to  $10^{-5}$  [22]. So far,  $I$ -VED has been successfully tested in different two-phase systems, as well as in a few in-vivo studies [22,24,25,27,28,30–34]. Electrical measurements are conducted with a pair of metallic ring electrodes (separation distance:  $D/4$ , electrode width:  $D/10$ ), which are flush-mounted to the inner walls of the vertical pipe, at an axial distance of 59 cm ( $\sim 28D$ ) from the gas injection point. This distance is almost double the necessary entrance length to ensure fully development of steady upward bubbly flow for the experimental conditions applied in this work ( $\sim 16D$ ) and, thus, is considered adequate for a fully developed pulsating flow as well [35]. Furthermore, it enables direct comparison of obtained results with those arisen from the corresponding experiments under steady flow conditions

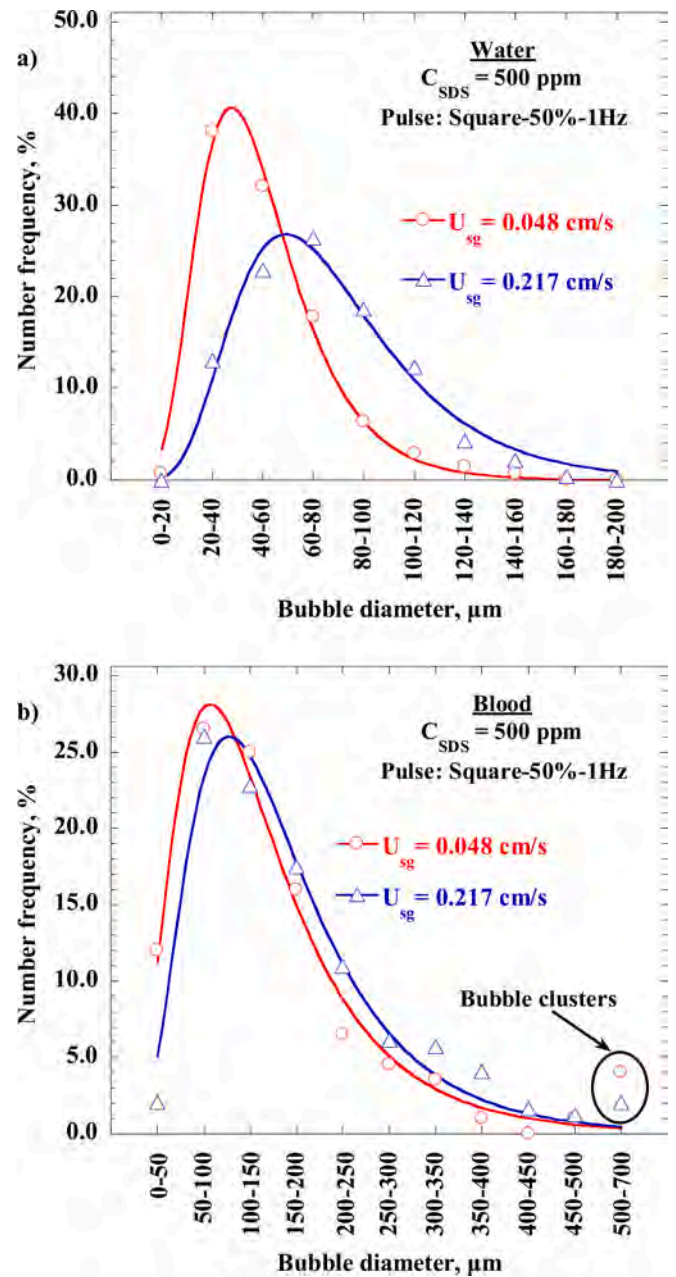


Fig. 5. Bubble Size Distributions for varying gas superficial velocity ( $U_{sg}$ ) in a) Water with  $C_{SDS} = 500$  ppm and b) Blood with  $C_{SDS} = 500$  ppm, when applying a square pulse with duty cycle 50 % and frequency 1 Hz to liquid flow (resulting  $U_{sl} = 2.89 \pm 0.96$  cm/s).

where  $I$ -VED measurements were performed at the same distance above the gas injection point ( $\sim 28D$ ) [22–25]. A sinusoidal voltage signal (frequency: 25 kHz, amplitude: 2 V<sub>p-p</sub>) is applied through the electrodes to excite electrically the bubbly flow and, then, a 24-bit data acquisition card (E-MU 1616 m, CREATIVE Professional) records the electrical signal with a sampling frequency of 192 kHz. Acquired  $I$ -VED signal is digitally processed and filtered by a custom Matlab routine, while the final output of data reduction is an electrical impedance time-series which is transformed to  $\epsilon$  time-series through Maxwell model [36]. More information about  $I$ -VED hardware and software operation can be found in [22].

$I$ -VED measurements are conducted synchronously with optical measurements for the estimation of BSD, based on a method described analytically in a previous study [22]. BSD determination is based on

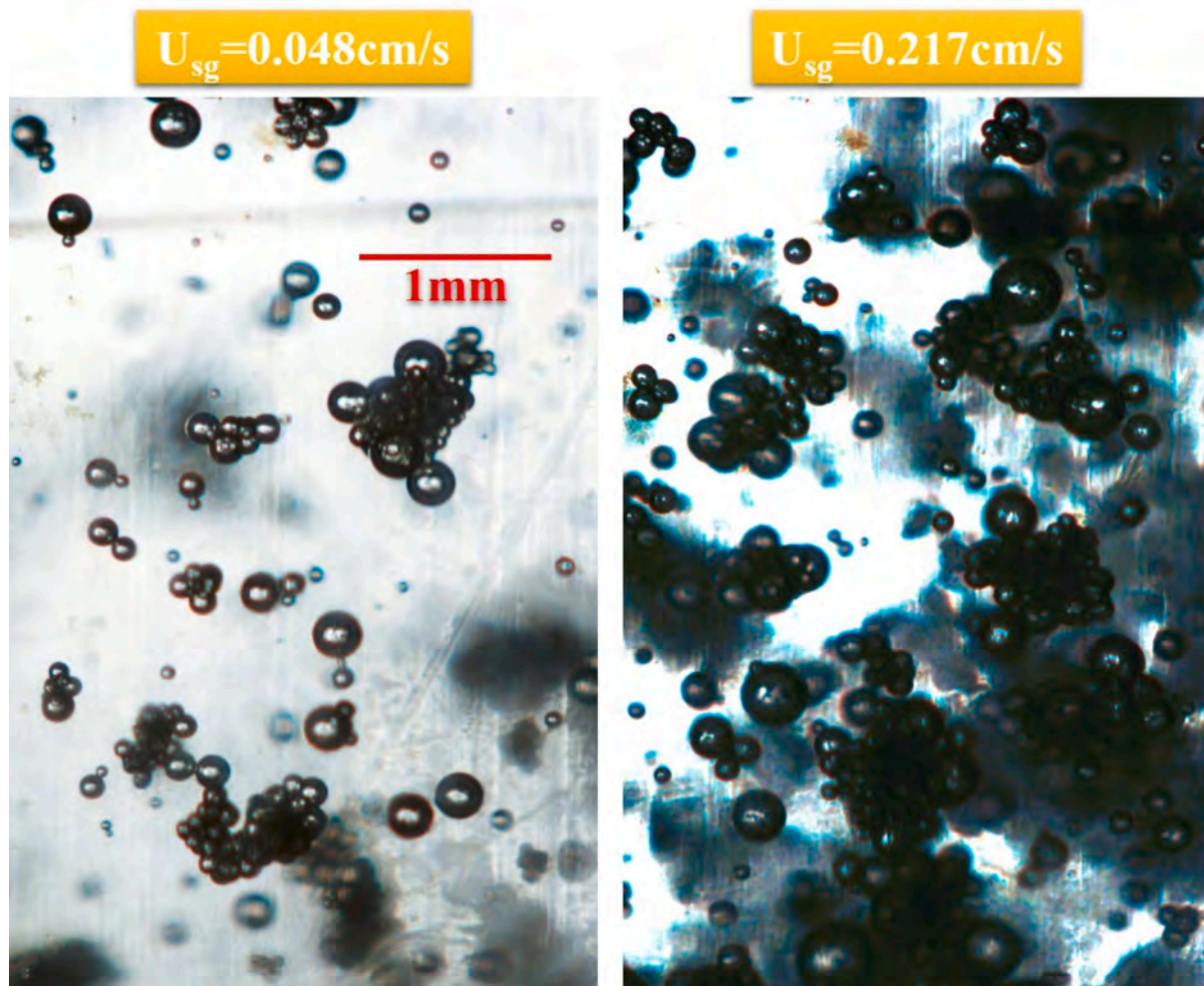


Fig. 6. Typical bubble clusters rising among isolated bubbles in Blood with  $C_{SDS} = 500$  ppm, when applying a square pulse with duty cycle 50 % and frequency 1 Hz to liquid flow (resulting  $U_{sl} = 2.89 \pm 0.96$  cm/s).

image processing of bubbly flow images captured at three radial positions inside the vertical tube ( $r = 0$ ,  $r = D/4$  and  $r = D/2$ ) at an axial distance of 75 cm ( $\sim 36D$ ) above the gas injection point. This distance equals to that applied for the optical measurements during the corresponding experiments under steady flow conditions to allow direct comparison of obtained results [22,23]. Images are recorded by CANON EOS 350D still digital camera, equipped with proper macro lens (CANON EF100mm, f/2.8 Macro USM) and extension rings (CANON, 13–21–31 mm). For each experimental run, an average *BSD* for the entire duration of flow pulsation is estimated employing a custom software (BubbleSEdit, [37]) that analyzes series of images accumulating 500–1000 bubbles to achieve good statistical significance [38]. Radial deviations have been shown minor in such conditions [39], so *BSDs* consist of bubbles from all radial positions. In agreement with relevant studies [40], two-parameter (scale and shape parameter) log-normal distribution fits adequately the *BSDs* resulted from image processing. For all *BSDs*, the arithmetic average bubble diameter,  $D_{1,0}$ , as well as the corresponding standard deviation,  $StDev(D_{1,0})$ , are computed and used in the next Section to describe the distributions instead of scale and shape parameter, respectively (scale and shape parameter designate the average and the standard deviation of the data after their logarithmic transformation, [23]).

Experiments are conducted with two different Newtonian test liquids, whose temperature is set to  $37.0 \pm 0.1$  °C (same as body temperature): a) an aqueous solution of NaCl 0.02 % w/w (purity > 99.5 %, Merck KGaA) that resembles the electrical conductivity of tap water,

hereafter called *Water* and b) an aqueous solution of NaCl 1.3 % w/w and glycerol 56.0 % w/w (purity > 99.5 %, Panreac) that simulates human blood physical properties, hereafter called *Blood* (electrical conductivity  $\sim 5.4$  mS/cm, dynamic viscosity 4–5 mPa.s, [41]). Although whole blood is a non-homogeneous complex liquid which exhibits non-Newtonian (shear-thinning) behavior due to red blood cells' shape alteration with shear rate, blood plasma is considered a Newtonian liquid. Consequently, as a first approximation of actual conditions, Newtonian liquids are usually used to simulate the rheological behavior of blood in literature [22,39,42]. Measured physical properties of both test liquids at 37 °C are given in Table 1.

Bubbles are generated by Helium gas (purity 99.9996 %, Air Liquide) due to its low solubility in the test liquids. Their size is controlled by adding the surface active agent Sodium Dodecyl Sulphate (*SDS*, purity > 99.0 %, Fluka Biochemika). Two bubble populations characterized by different average bubble sizes, both below 1 mm as those encountered in *DCS* incidents [29], are examined for each test liquid. It was preliminary shown that fairly distinct *BSDs* result from the following applied concentration values of *SDS*:  $C_{SDS} = 5$  ppm and  $C_{SDS} = 500$  ppm in *Water*,  $C_{SDS} = 0$  ppm and  $C_{SDS} = 500$  ppm in *Blood*.

All experiments are conducted for the same average liquid superficial velocity,  $U_{sl} = 2.89$  cm/s, which is in the range of blood velocities noticed in human vena cava [29]. However,  $U_{sl}$  fluctuations around its mean value vary with the employed flow pulsation type and duty cycle:  $2.89 \pm 0.33$  cm/s for square pulse with duty cycle 80 %,  $2.89 \pm 0.96$  cm/s for square pulse with duty cycle 50 %,  $2.89 \pm 1.30$  cm/s for square

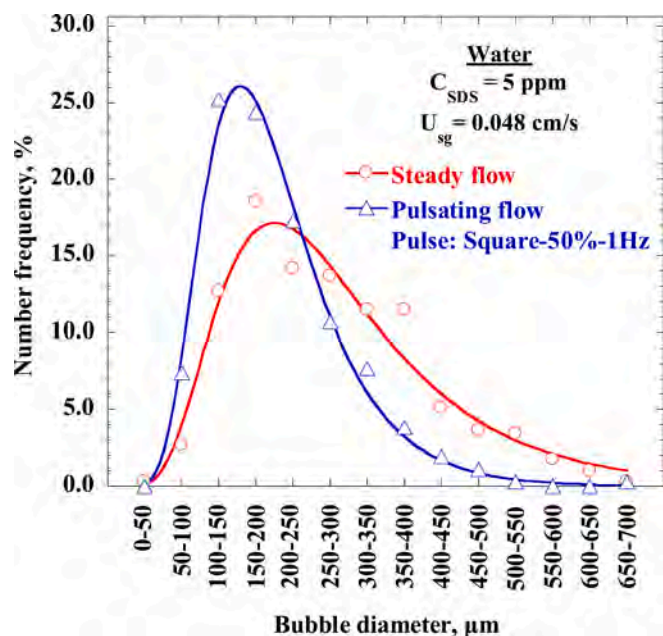


Fig. 7. Comparison of Bubble Size Distributions between steady flow and single-phase pulsating flow (square pulse with duty cycle 50 % and frequency 1 Hz) for  $U_{sl} = 2.89$  cm/s and  $U_{sg} = 0.048$  cm/s, in Water with  $C_{SDS} = 5$  ppm.

pulse with duty cycle 30 % and  $2.89 \pm 0.76$  cm/s for sinusoidal pulse. Accordingly, Reynolds number of liquid phase ( $Re$ ) fluctuates between 860 and 1450 in Water and between 80 and 200 in Blood, implying always laminar flow conditions. Pulse frequency is set to 1 Hz, which corresponds to 60 beats/min heart rate. On the other hand, we examine three different gas superficial velocities,  $U_{sg} = 0.048$ – $0.217$ – $0.385$  cm/s, that provide void fraction values from  $10^{-3}$  to  $10^{-1}$ . Although  $\varepsilon$  values larger than 0.05 are not encountered in typical DCS incidents, they contribute to study completeness. Applied  $U_{sl}$  and  $U_{sg}$  values result always in bubbly flow pattern, according to the map of Taitel *et al.* [43].

### 3. Results and discussion

It is well-known that void fraction inside a vessel strongly depends on the size of bubbles. Thus, we describe first the influence of different parameters on  $BSD$  features in order to facilitate the discussion on void fraction variation for the examined conditions that follows.

#### 3.1. Bubble size distribution

As explained in the previous Section, the arithmetic average bubble diameter,  $D_{1,0}$ , and the corresponding standard deviation,  $StDev(D_{1,0})$ , can describe adequately a log-normal  $BSD$ . For this, Figs. 2 and 3 present the effect of  $C_{SDS}$  and gas superficial velocity,  $U_{sg}$ , on  $D_{1,0}$  and  $StDev(D_{1,0})$  of  $BSDs$  in Water and Blood, when applying a square pulse with a duty cycle 50 % and frequency 1 Hz to liquid flow. For study completeness reasons, the  $BSDs$  for both test liquids and SDS concentrations are given in Figs. 4 and 5 ( $U_{sg} = 0.048$  cm/s and  $0.217$  cm/s). Fig. 2a and 3a show that  $D_{1,0}$  lowers significantly for  $C_{SDS} = 500$  ppm in both liquids, due to the reduction of liquid surface tension (Table 1) and the inhibition of bubbles coalescence induced by the restriction of bubble surface mobility as a result of surfactant molecules adsorption at the bubble interface [44]. Concerning the influence of liquid physical properties on  $D_{1,0}$ , it is interesting to notice that:

a)  $D_{1,0}$  values do not differ between Water in the presence of surfactant ( $C_{SDS} = 5$  ppm) and Blood in the absence of surfactant, Fig. 2a, because bubbles coalescence is already prevented in Blood by the increased concentration of NaCl (1.3 % w/w) [22,45].

b) For  $C_{SDS} = 500$  ppm, bubbles in Blood are larger than those in Water (comparing red and blue circular points in Fig. 3a). This is attributed to bubble clusters with an equivalent diameter ranging from 500 to 700  $\mu\text{m}$  that rise inside the pipe among isolated bubbles, Fig. 6. Bubble clusters are formed due to the synergistic action of glycerol that increases liquid viscosity (Table 1), NaCl and SDS, while the physico-chemical interactions that lead to their production have been previously described in details [23]. However, isolated bubbles in Blood are still larger than those in Water (comparing red triangular points with blue circular points in Fig. 3a). This means that the increased number of bubbles' collisions in Blood, due to the higher liquid viscosity that retards bubbles movement, does not result exclusively in the formation of clusters but in several coalescence events as well.

As expected,  $StDev(D_{1,0})$  decreases with  $C_{SDS}$  increase in Water, Fig. 2b and 3b. On the contrary, the addition of 500 ppm SDS in Blood increases  $StDev(D_{1,0})$  for  $U_{sg} = 0.048$  cm/s, does not change  $StDev(D_{1,0})$  for  $U_{sg} = 0.217$  cm/s and decreases  $StDev(D_{1,0})$  only for  $U_{sg} = 0.385$  cm/s, Fig. 2b and 3b. This behavior is caused again by the bubble clusters that affect  $StDev(D_{1,0})$  much more than  $D_{1,0}$ , while their contribution to  $BSD$  features minimizes with  $U_{sg}$  increase.

$D_{1,0}$  increases with  $U_{sg}$  for both liquids and  $C_{SDS}$  values, Fig. 2a and Fig. 3a, due to: a) Greater growth of bubbles before their detachment from the pores of the glass filter and b) Production of more bubbles that increases collision frequency and, as a result, coalescence phenomena. This behavior has been also noticed in other studies [23,46].  $StDev(D_{1,0})$  dependence on  $U_{sg}$  is similar (Fig. 2b and Fig. 3b), except for  $C_{SDS} = 500$  ppm in Blood where the ratio  $\frac{\text{Number of bubble clusters}}{\text{Number of isolated clusters}}$  reduces with the increase of  $U_{sg}$  and leads to  $StDev(D_{1,0})$  decrease as well (red circular points in Fig. 3b).

Based on the above, the influence of gas superficial velocity, surfactant concentration and liquid properties on  $BSD$  features does not differ qualitatively between pulsating and steady flow conditions. It is of great interest, however, to investigate whether pulsating flow conditions affect by themselves the average bubble diameter and the corresponding standard deviation of  $BSDs$  under study. Keeping all the experimental conditions unaltered (test liquids, surfactant concentrations and gas/liquid superficial velocities) except for the flow type (steady-[22] vs pulsating-current study), it is shown that  $D_{1,0}$  decreases when employing pulsating flow conditions. In the most cases, this reduction ranges from 2 % to 15 % and is within the limits of experimental/statistical error. In Water with  $C_{SDS} = 5$  ppm, however,  $D_{1,0}$  decreases  $\sim 25$  % for all  $U_{sg}$  values and this can be attributed to the pulsating flow conditions that cause disintegration of large bubbles into smaller ones. Indicatively, Fig. 7 compares the  $BSDs$  between steady flow and single-phase pulsating flow (square pulse with duty cycle 50 % and frequency 1 Hz) for  $U_{sl} = 2.89$  cm/s and  $U_{sg} = 0.048$  cm/s. In literature, Abishek *et al.* [1] have also noticed bubbles breakup induced by pulsating flow, but for different flow pattern (slug) and liquid type (non-Newtonian). Such an effect cannot be found in the other cases of this study since bubbles are already small prior to pulsating flow conditions application, due to high concentration of SDS or NaCl that prevents bubbles coalescence. As concerns  $StDev(D_{1,0})$ , it is significantly decreased not only in Water with  $C_{SDS} = 5$  ppm ( $\sim 30$  %), but also in Blood with  $C_{SDS} = 500$  ppm ( $\sim 40$  %) where pulsating flow conditions make voluminous bubble clusters disintegrate into smaller ones or isolated bubbles. In Water with  $C_{SDS} = 500$  ppm and in Blood without SDS addition, on the other hand,  $StDev(D_{1,0})$  can either decrease or increase within the limits of experimental/statistical error.

#### 3.2. Void fraction

##### 3.2.1. Single-phase (liquid) pulsating flow

Figs. 8 and 9 present void fraction ( $\varepsilon$ ) time-series for three  $U_{sg}$  values (0.048 – 0.217 – 0.385 cm/s) and two  $C_{SDS}$  values (5 or 0 ppm and 500 ppm) in Water and Blood. In all cases, a square pulse with duty cycle 50

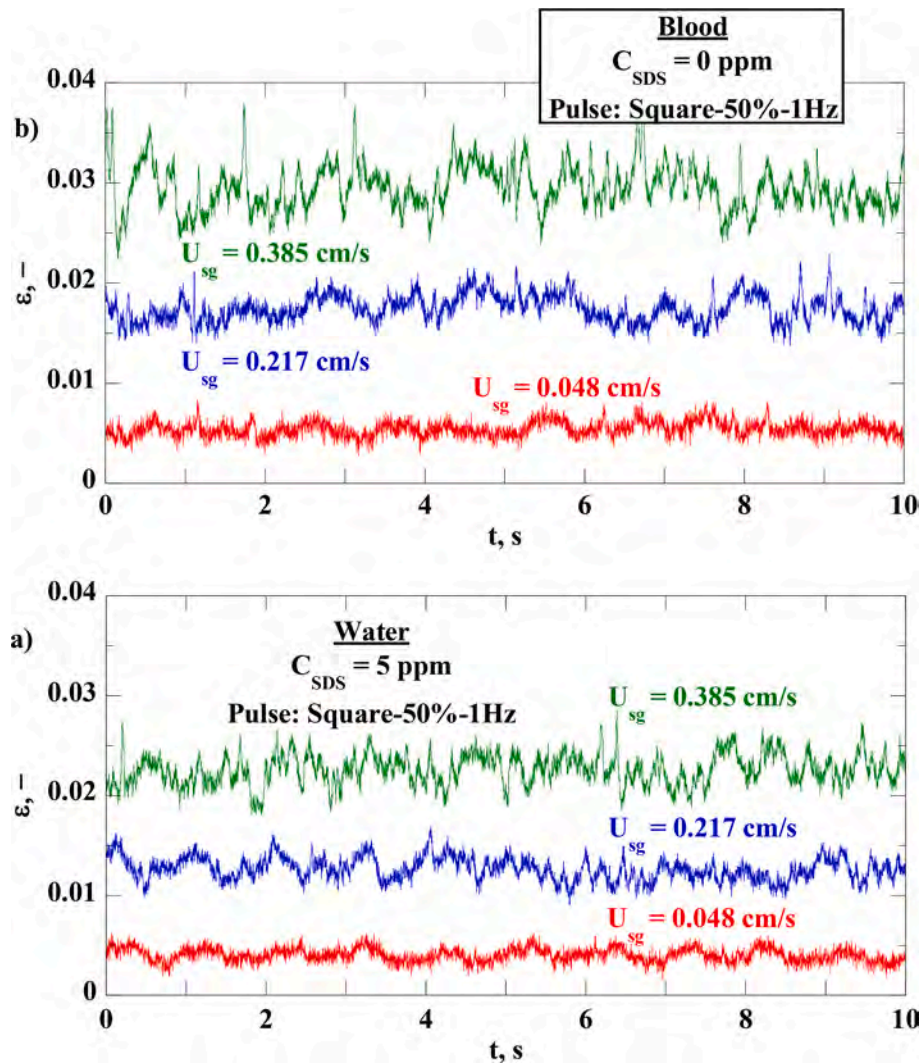


**Fig. 8.** Void fraction ( $\epsilon$ ) time-series for varying gas superficial velocity ( $U_{sg}$ ) in a) Water with  $C_{SDS} = 5$  ppm and b) Blood with  $C_{SDS} = 0$  ppm, when applying a square pulse with duty cycle 50 % and frequency 1 Hz to liquid flow (resulting  $U_{sl} = 2.89 \pm 0.96$  cm/s).

% and frequency 1 Hz is employed to liquid flow resulting in  $U_{sl} = 2.89 \pm 0.96$  cm/s. First, we discuss the effect of different parameters on average  $\epsilon$  value and then on signal fluctuations. Average void fraction increases with  $U_{sg}$  in both liquids, as expected, since gas volumetric concentration inside the vertical pipe gets higher. Nevertheless, the increase is not linear with  $U_{sg}$  because, apart from gas flow rate, the size of bubbles also plays role (Figs. 2 and 3). Average void fraction increases with  $C_{SDS}$  as well, since bubbles become smaller and their residence time inside the vertical pipe increases due to decreasing buoyant velocity [47]. The influence of liquid properties on average  $\epsilon$  can be clearly shown by comparing  $\epsilon$  signals in Water with  $C_{SDS} = 5$  ppm, Fig. 8a, with those in Blood with  $C_{SDS} = 0$  ppm, Fig. 8b, because bubble sizes are similar. For all  $U_{sg}$  values, average void fraction increases in Blood since it is  $\sim 7$  times more viscous than Water and makes bubbles rising with lower velocity inside the vertical pipe increasing their residence time. Again, the variation is not linear with liquid viscosity because the size of bubbles matters, too. For  $C_{SDS} = 500$  ppm, on the contrary, void fraction decreases in Blood due to voluminous bubble clusters which buoyancy makes rise faster than single bubbles do in Water despite the increased viscosity. Finally, average void fraction values differ less than 10 % between steady [22] and pulsating flow (current study) for similar experimental conditions. Consequently, liquid flow conditions do not show any considerable effect on the mean  $\epsilon$  and this is explained by the fact that liquid pulsating flow does not change mean liquid superficial

velocity and hardly lowers – occasionally - bubble size.

Void fraction signal fluctuations are intensified with increasing  $U_{sg}$  and decreasing  $C_{SDS}$ , because bubbles become larger and cause greater disturbances of the electric field as they cross the measuring volume between the two electrodes. Interestingly, void fraction signals in Water with  $C_{SDS} = 500$  ppm show a periodic fluctuation every 1 s, Fig. 9a, which is undoubtedly related with the liquid flow pulsation of 1 Hz and may be so evident because bubbles travel with liquid velocity (Stokes terminal velocity of bubbles with  $D_{1,0}$  ranging from about 25  $\mu\text{m}$  to 100  $\mu\text{m}$ , Fig. 3, is much lower than the average  $U_{sl}$  value, namely, from 0.05 cm/s to 0.75 cm/s). The amplitude of this fluctuation increases with gas superficial velocity. In Blood with  $C_{SDS} = 500$  ppm, on the other hand, bubble clusters rising among isolated bubbles disturb significantly the electric field and also travel faster than the liquid (Stokes terminal velocity of bubble clusters with equivalent diameter from 500  $\mu\text{m}$  to 700  $\mu\text{m}$  ranges from 3 cm/s to 6 cm/s). As a result, the repeatable fluctuation becomes less distinguishable, Fig. 9b. For the low  $C_{SDS}$  value in Water, 5 ppm, bubbles are large enough to cause intense electric field disturbances and accelerate with regards to the liquid phase, since Stokes terminal velocity of bubbles with  $D_{1,0}$  from about 120  $\mu\text{m}$  to 450  $\mu\text{m}$ , Fig. 2, ranges from 1 cm/s to 15 cm/s. Consequently, such large bubbles mask macroscopically void fraction fluctuations related with the liquid flow pulsation, Fig. 8a. In Blood without the addition of SDS surfactant, bubbles ascend more or less with liquid velocity (Stokes terminal



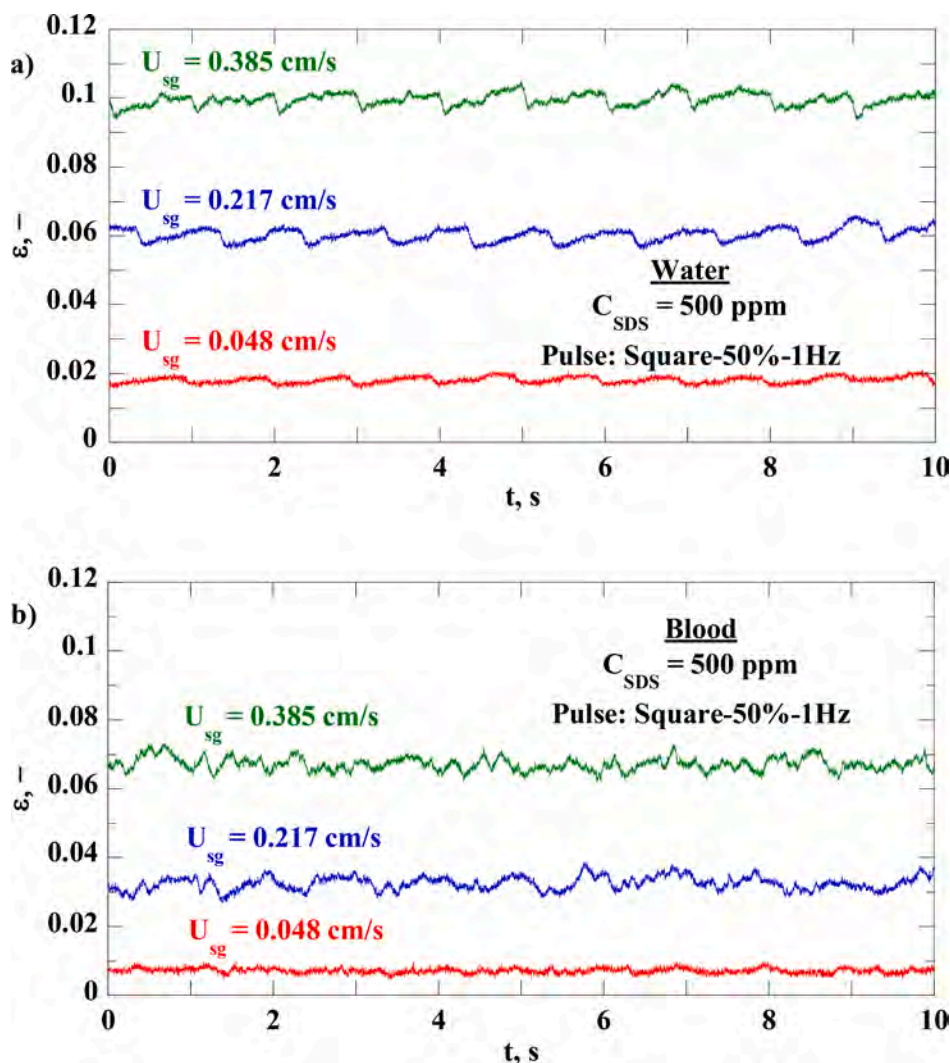


Fig. 9. Void fraction ( $\epsilon$ ) time-series for varying gas superficial velocity ( $U_{sg}$ ) in a) Water with  $C_{SDS} = 500$  ppm and b) Blood with  $C_{SDS} = 500$  ppm, when applying a square pulse with duty cycle 50 % and frequency 1 Hz to liquid flow (resulting  $U_{sl} = 2.89 \pm 0.96$  cm/s).

velocity of bubbles with  $D_{1,0}$  from about 120  $\mu\text{m}$  to 450  $\mu\text{m}$ , Fig. 2, ranges from 0.2 cm/s to 2.5 cm/s), however void fraction periodic fluctuation every 1 s is again non-recognizable, Fig. 8b). This can be attributed to Blood's augmented viscosity that retards the rise of bubbles and increases the population of large bubbles (due to the absence of surfactant) that cross the area between the electrodes causing intense signal fluctuations. FFT spectral analysis of obtained void fraction signals (Figs. 10 and 11), nevertheless, reveals a hidden periodicity of 1 Hz for  $U_{sg} = 0.048$  cm/s in Water with  $C_{SDS} = 5$  ppm (Fig. 10a) and in Blood with  $C_{SDS} = 0$  ppm (Fig. 10b), as well as in Blood with  $C_{SDS} = 500$  ppm for  $U_{sg} = 0.048$  cm/s and 0.217 cm/s (Fig. 11b).

### 3.2.2. Two-phase (gas–liquid) pulsating flow

Fig. 12 compares the influence of three different two-phase (gas–liquid) pulsating flow types on synchronized void fraction and relative pressure signals, for  $U_{sg} = 0.217$  cm/s in Water with  $C_{SDS} = 500$  ppm. Electrical and relative pressure measurements (PT-2 in Fig. 1) are conducted at an axial distance of 59 cm and 53 cm from the gas injection point respectively and, therefore, void fraction signals show a small delay with respect to pressure ones. The employed pulse types are the following: a) square pulse with duty cycle 80 % and frequency 1 Hz resulting in  $U_{sl} = 2.89 \pm 0.33$  cm/s, b) square pulse with duty cycle 30 % and frequency 1 Hz resulting in  $U_{sl} = 2.89 \pm 1.30$  cm/s and c) sinusoidal pulse with frequency 1 Hz resulting in  $U_{sl} = 2.89 \pm 0.76$  cm/s. The

application of square pulse with duty cycle 80 % (valve is open for 80 % of a single pulse duration) to the two-phase flow is close enough to steady flow and, consequently, the periodic fluctuation of 1 Hz cannot be distinguished in the void fraction signal (red line in Fig. 12a). Yet, the pulse is clearly depicted in the corresponding pressure signal (red line in Fig. 12b). On the contrary, the periodic fluctuation of 1 Hz is clearly noticed in both void fraction and pressure signals, when employing the sinusoidal pulse and the square pulse with duty cycle 30 % (blue and green lines in Fig. 12a and b). This is explained as follows: As valve closes for longer time, it interrupts the two-phase flow along the vertical pipe for longer time as well. Thus, the number of bubbles above the valve decreases significantly and numerous bubbles are trapped at the rear part of the valve. Accordingly, the measured void fraction above the valve decreases, too. However, as soon as the valve opens and lets bubbles rise in the vertical pipe with the liquid flow, void fraction increases rapidly. The amplitude of void fraction and pressure signals increases with duty cycle reduction, while during a single cycle both void fraction and relative pressure take their maximum values when the valve is fully open. Additionally, it is interesting to observe the following void fraction signal features:

- Average void fraction increases inversely to duty cycle, Fig. 12a. This feature indicates a possible controlled increase of void fraction, thus of gas–liquid interfacial area, by proper tuning of pulsation

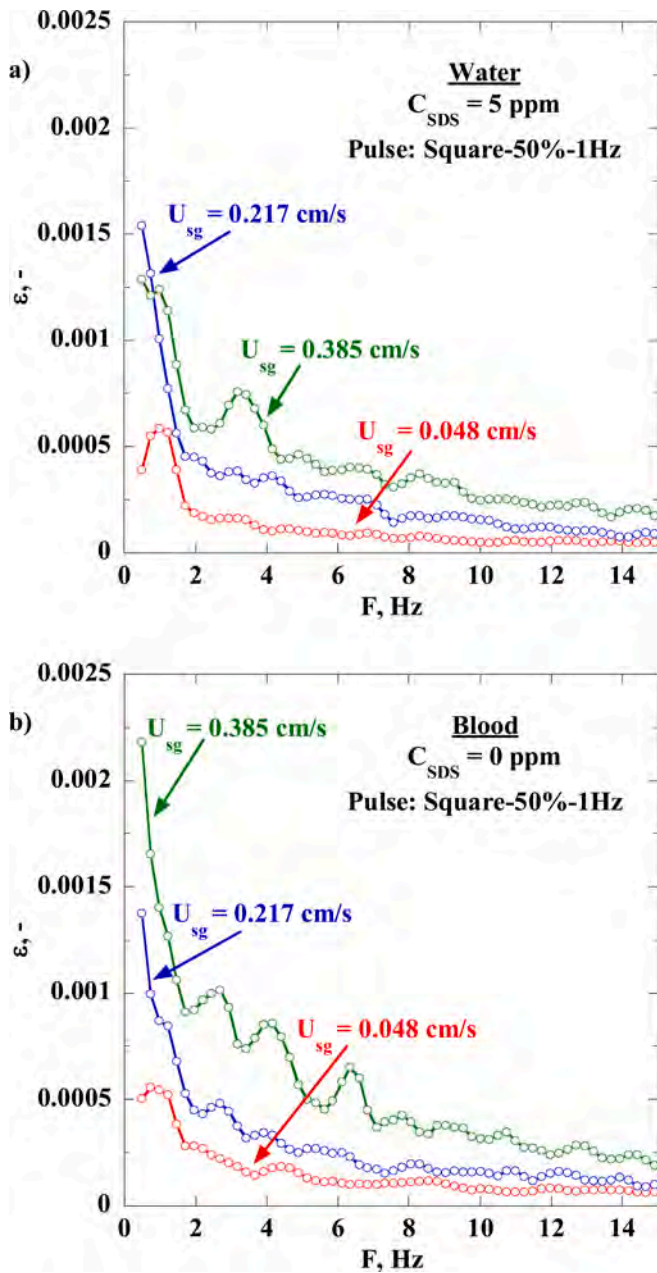


Fig. 10. FFT spectra of void fraction ( $\epsilon$ ) time-series for varying gas superficial velocity ( $U_{sg}$ ) in a) Water with  $C_{SDS} = 5$  ppm and b) Blood with  $C_{SDS} = 0$  ppm, when applying a square pulse with duty cycle 50 % and frequency 1 Hz to liquid flow (resulting  $U_{sl} = 2.89 \pm 0.96$  cm/s).

conditions. It is noteworthy that a duty cycle 30 % leads to a *BSD* which is considerably more intense in the size class 60–80  $\mu\text{m}$  and notably less intense in the size classes from 100 to 140  $\mu\text{m}$  as compared to a duty cycle 80 % and a sinusoidal pulse (Fig. 12c). Smaller bubbles undoubtedly yield higher void fractions. However, void fraction increase might be also associated with the complexity of two-phase flow field due to the severity of a low pulsation duty cycle. Specifically, for a square pulse with duty cycle 30 %, liquid superficial velocity fluctuates periodically between  $2.89 \pm 1.30$  cm/s, which is the highest disturbance observed in this study. It is quite probable that such fluctuations cause intense transient accelerations and decelerations of the flow in the pipe center (the orifice of valve is 5 mm smaller than the pipe diameter,  $D = 21$  mm) and subsequent flow reverse (recirculation) close to the pipe wall. As a result, the residence time of bubbles close to the pipe wall increases

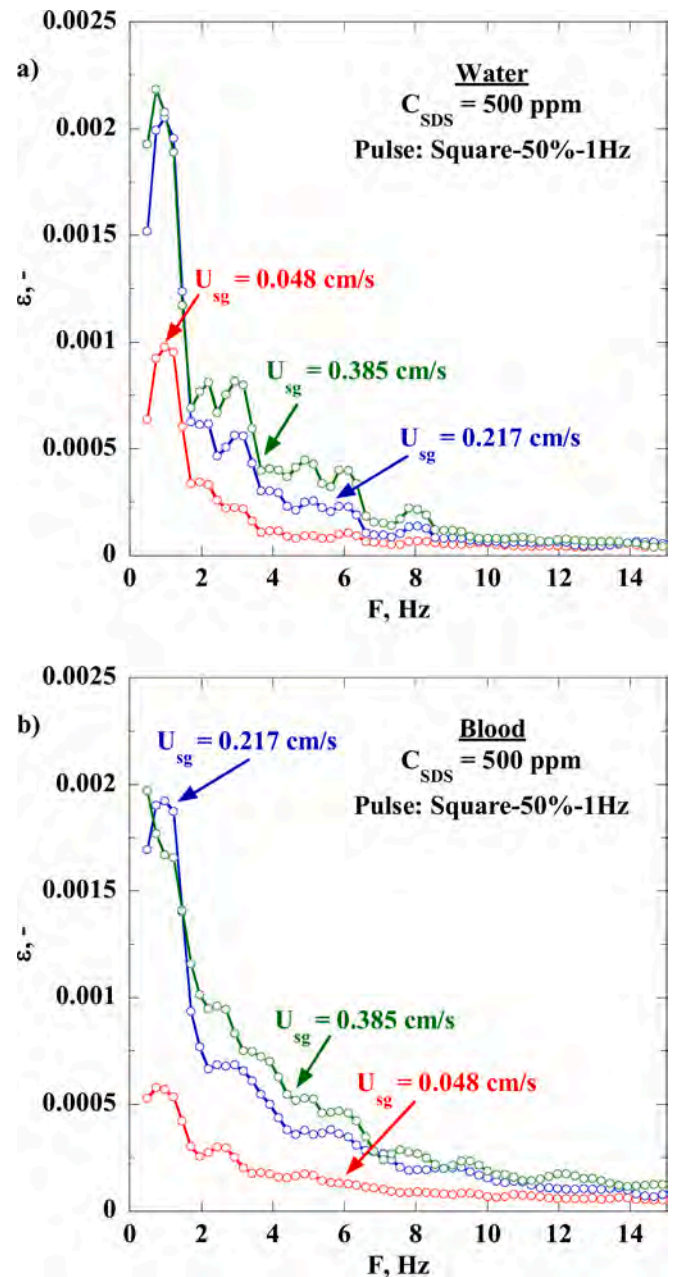


Fig. 11. FFT spectra of void fraction ( $\epsilon$ ) time-series for varying gas superficial velocity ( $U_{sg}$ ) in a) Water with  $C_{SDS} = 500$  ppm and b) Blood with  $C_{SDS} = 500$  ppm, when applying a square pulse with duty cycle 50 % and frequency 1 Hz to liquid flow (resulting  $U_{sl} = 2.89 \pm 0.96$  cm/s).

considerably (buoyancy does not practically affect such small bubbles) and leads to void fraction increase at a longitudinal distance of  $\sim 21D$  above the valve position where measurements takes place. However, it is doubtful whether lowering continually the duty cycle will monotonically increase the average void fraction; the time percentage of the pulse duration where the valve is open will decrease accordingly and may be not enough to let the majority of the trapped bubbles at the rear part of the valve pass through this and rise in the vertical pipe. It is expected that there is a threshold in low duty cycle, below which void fraction does not increase any more. In any case, the noticed trend of average void fraction increase with the decrease of flow pulsation duty cycle may benefit several industrial applications by enhancing gas–liquid mass transfer through gas–liquid interfacial area increase.

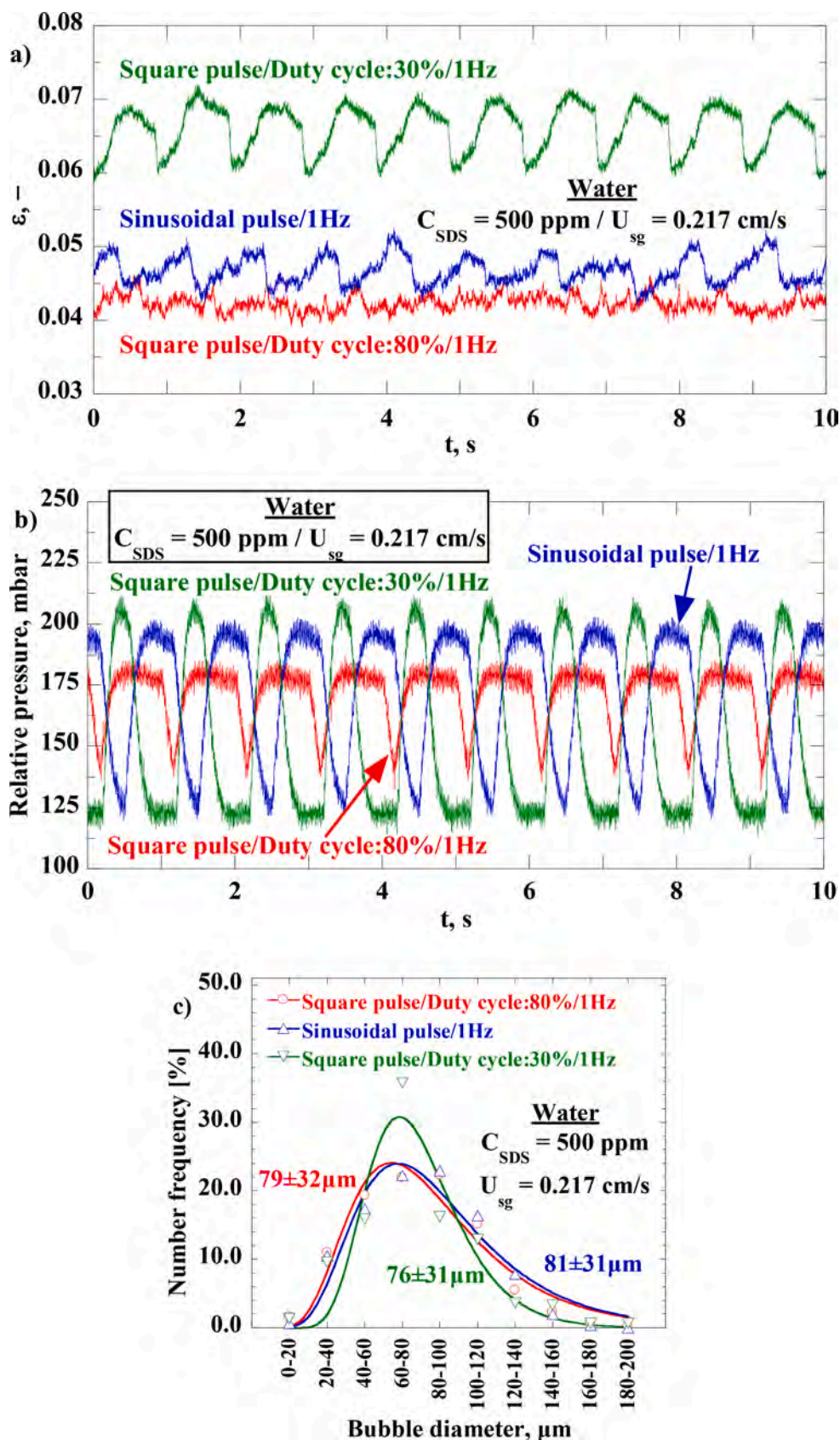
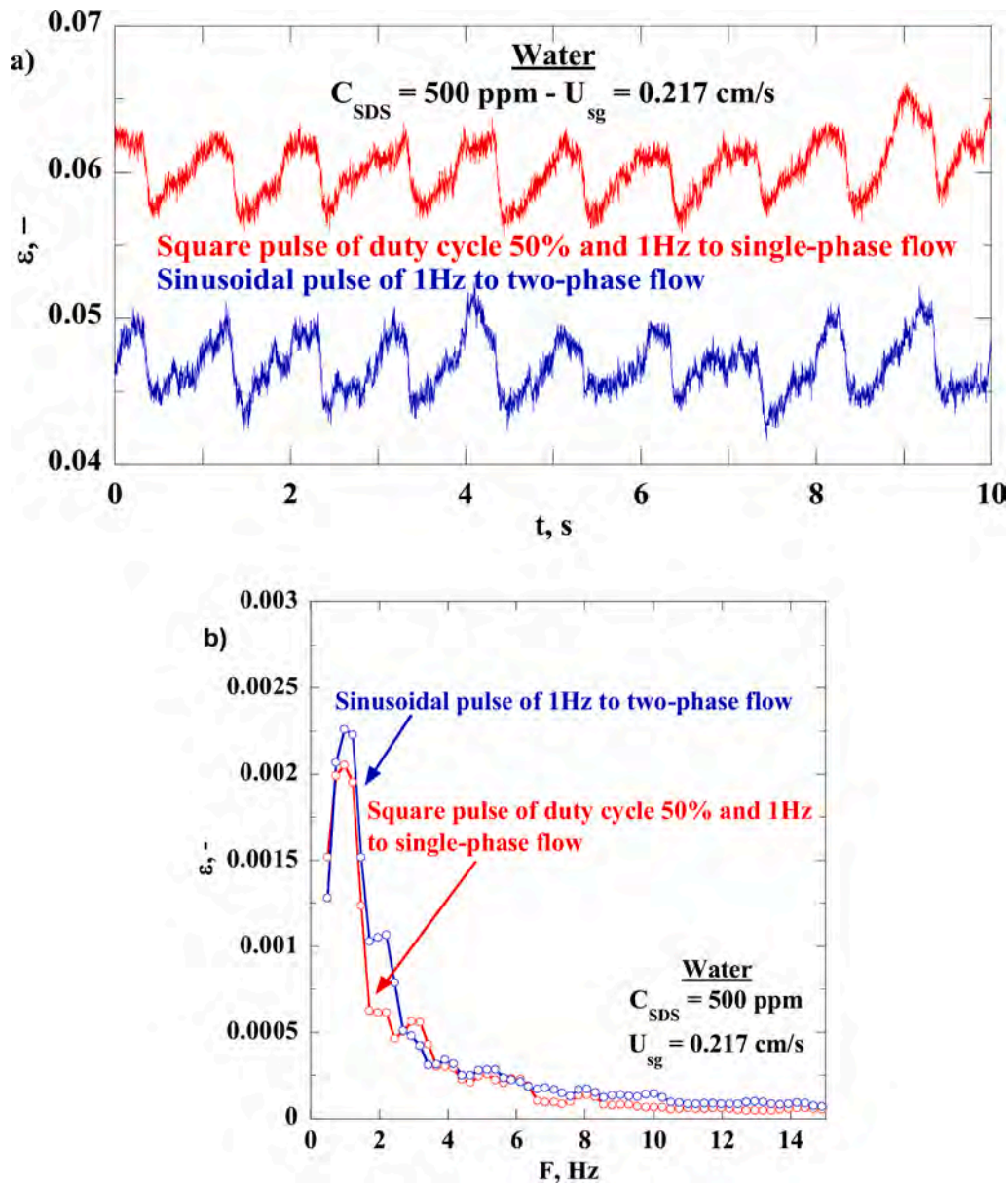


Fig. 12. a) Void fraction ( $\epsilon$ ) time-series, b) relative pressure time-series and c) Bubble Size Distributions for  $U_{sg} = 0.217 \text{ cm/s}$  in Water with  $C_{SDS} = 500 \text{ ppm}$ , employing three different pulse types with frequency 1 Hz to two-phase flow: i) square pulse with duty cycle 80 % resulting in  $U_{sl} = 2.89 \pm 0.33 \text{ cm/s}$ , b) square pulse with duty cycle 30 % resulting in  $U_{sl} = 2.89 \pm 1.30 \text{ cm/s}$  and c) sinusoidal pulse resulting in  $U_{sl} = 2.89 \pm 0.76 \text{ cm/s}$ .



**Fig. 13.** Comparison of a) Void fraction ( $\epsilon$ ) time-series and b) Corresponding FFT spectra between two different pulsating flow types: Sinusoidal pulse of 1 Hz to two-phase flow ( $U_{sl} = 2.89 \pm 0.76 \text{ cm/s}$ ) vs square pulse of duty cycle 50 % and 1 Hz to single-phase flow ( $U_{sl} = 2.89 \pm 0.96 \text{ cm/s}$ ), for  $U_{sg} = 0.217 \text{ cm/s}$  in Water with  $C_{SDS} = 500 \text{ ppm}$ .

- b) The smoothness of void fraction increase/decrease during a cycle varies with applied pulse type: Sinusoidal pulse causes pretty smooth fluctuations, while square pulse with duty cycle 30 % makes fluctuations much steeper and for this reason square pulse seems more pronounced.
- c) Void fraction signal variation when applying sinusoidal pulse to two-phase flow, as estimated by the standard deviation which is 0.0019, equals to that when employing square pulse with duty cycle of 50 % to liquid flow solely, Fig. 13a. Also, FFT spectra of void fraction signals are alike in these two cases, Fig. 13b: a) Spectrum decay at  $\sim 6 \text{ Hz}$  and b) Spectrum peak around  $\epsilon = 0.002$  at 1 Hz. Since the two pulse types are alike, it is demonstrated that signal characteristics do not differ between single-phase and two-phase pulsating flow conditions. However, average void fraction is lower in the case of two-phase pulsating flow because the valve interrupts not only the liquid flow but the gas flow as well.

Finally, FFT spectra of void fraction time-series presented in Fig. 12a

clearly show a dominant peak at 1 Hz, even for the case of square pulse with duty cycle 80 % where such a periodicity could not be macroscopically detected in the original signal, Fig. 14.

#### 4. Conclusions

This work studies void fraction and bubble size in a pulsating gas-liquid flow of sub-mm bubbles at low void fractions ( $< 10^{-1}$ ), that resembles bubbly flow in human vena cava during Decompression Sickness and is also encountered in conventional activated sludge systems for municipal sewage treatment despite the different local characteristics. Experiments are performed in a vertical co-current upward bubbly flow provided by a fully controllable flow loop, which can generate pulsating conditions of varying frequency, amplitude and profile both in liquid and gas-liquid flow. Void fraction is measured with a highly-sensitive electrical impedance spectroscopy technique, while BSD is determined by performing advanced image processing on bubbly flow images. Experiments are conducted in water and blood simulant,

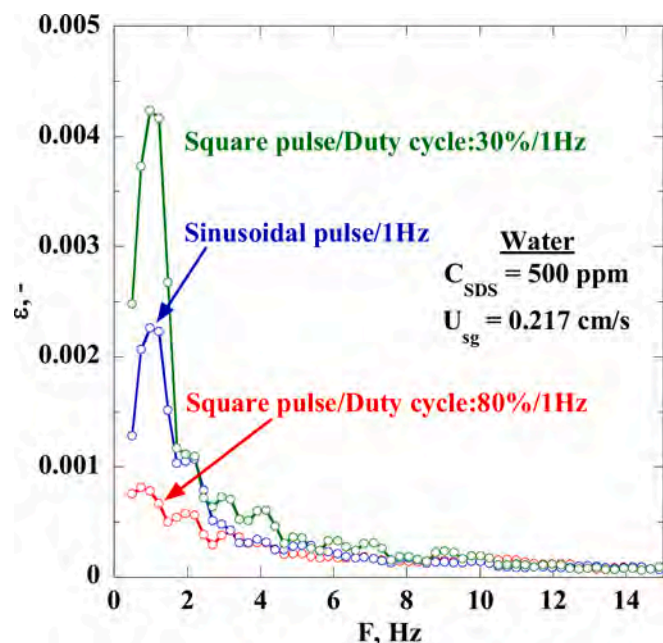



Fig. 14. FFT spectra of void fraction ( $\epsilon$ ) time-series for  $U_{sg} = 0.217$  cm/s in Water with  $C_{SDS} = 500$  ppm, employing three different pulse types with frequency 1 Hz to two-phase flow: i) square pulse with duty cycle 80 % resulting in  $U_{sl} = 2.89 \pm 0.33$  cm/s, b) square pulse with duty cycle 30 % resulting in  $U_{sl} = 2.89 \pm 1.30$  cm/s and c) sinusoidal pulse resulting in  $U_{sl} = 2.89 \pm 0.76$  cm/s.

while bubble size varies employing prescribed surfactant (SDS) concentrations. Bubble size increases with gas superficial velocity and decreases with surfactant addition that prevents bubbles coalescence. The synergistic action of increased viscosity and salinity in blood simulant along with the high surfactant concentration (500 ppm) results in the formation of bubble clusters (equivalent diameter: 500–700  $\mu\text{m}$ ) rising among isolated bubbles. Interestingly, pulsating flow conditions disintegrate: a) several clusters reducing their number comparing to steady flow and b) bubbles in water with the low surfactant concentration (5 ppm) reducing their size with regards to steady flow. As a result, proper tuning of pulsating flow conditions may enhance gas–liquid mass transfer in industrial applications due to induced gas–liquid interfacial area increase. On the other hand, average void fraction increases with gas superficial velocity, surfactant concentration that reduces bubble size and liquid viscosity (for equally sized bubbles) that augments the residence time of bubbles in the pipe. Compared to steady flow conditions, average void fraction remains almost unaltered when employing single-phase (liquid) pulsating flow and decreases with the application of two-phase (gas–liquid) pulsating flow. A periodic fluctuation of 1 Hz, related with pulsating conditions either in liquid or in gas–liquid flow, is clearly noticed in void fraction signals for bubbles from 25  $\mu\text{m}$  to 100  $\mu\text{m}$  that travel with the liquid velocity, however larger bubbles (120–450  $\mu\text{m}$ ) and bubble clusters disturb significantly the electric field between the applied electrodes and, consequently, mask macroscopically this pulsation. Moreover, both the amplitude of void fraction periodic fluctuation and the spectral content of electrical signals do not differ between single-phase and two-phase pulsating flow conditions when employing comparable pulsations. Testing different pulse types, finally, it is concluded that: a) the amplitude of void fraction signals increases with the reduction of pulsation duty cycle (time percentage where valve is open during a single pulse) and b) sinusoidal pulse causes smoother void fraction variation during a cycle than the square pulse. Evidence is provided that lowering the duty cycle yields higher void fraction and consequently gas–liquid interfacial area. This might be because flow pulsations lead on one hand to pretty smaller bubbles, due to bubbles breakage, and on the other hand to recirculation loops, i.e. reverse

(downward) flow, near the wall of the tube where mostly small bubbles reside to which buoyancy has minimal effect. The latter may have a great significance in process intensification regarding mass transfer through bubbly flows.

## Funding

This work was supported by  (GSTP Project: In-Vivo Embolic Detector, I-VED - Contract No.: 4000101764 and MAP Project: Convective boiling and condensation local analysis and modelling of dynamics and transfers, MANBO – Contract No.: 4200020289). The view expressed herein can in no way be taken to reflect the official opinion of the European Space Agency.

## CRedit authorship contribution statement

**Sotiris P. Evgenidis:** Writing – review & editing, Writing – original draft, Visualization, Validation, Software, Methodology, Investigation, Formal analysis, Data curation, Conceptualization. **Thodoris D. Karapantsios:** Writing – review & editing, Supervision, Project administration, Funding acquisition, Conceptualization.

## Declaration of competing interest

The authors declare that they have no known competing financial interests or personal relationships that could have appeared to influence the work reported in this paper.

## Data availability

Data will be made available on request.

## References

- [1] S. Abishek, A.J.C. King, R. Narayanaswamy, Dynamics of a Taylor bubble in steady and pulsatile co-current flow of newtonian and shear-thinning liquids in a vertical tube, *Int. J. Multiphas. Flow* 74 (2015) 148–164.
- [2] K. Haddad, O. Ertunc, M. Mishra, A. Delgado, Pulsating laminar fully developed channel and pipe flows, *Phys. Rev. E* 81 (2010) 016303.
- [3] W. Augustin, M. Bohnet, Influence of a pulsating flow on fouling behaviour of heat transfer surfaces, *Chem. Ing. t.* 73 (9) (2001) 1139–1144.
- [4] M.R. Khadilkar, M.H. Al-Dahhan, M.P. Dudukovic, Parametric study of unsteady-steady flow modulation in trickle-bed reactors, *Chem. Eng. Sci.* 54 (1999) 2585–2595.
- [5] P. Yang, Y. Zhang, X. Wang, Y. Liu, Heat transfer measurement and flow regime visualization of two-phase pulsating flow in an evaporator, *Int. J. Heat Mass Transf.* 127 (2018) 1014–1024.
- [6] H. Chen, Z. Yu, S. Bai, H. Lu, D. Xu, C. Chen, D. Liu, Y. Zhu, Microfluidic models of physiological or pathological flow shear stress for cell biology, disease modeling and drug development, *trends, Anal. Chem.* 117 (2019) 186–199.
- [7] A. Helgenland, K.A. Mardal, V. Haughton, B.A.P. Reif, Numerical simulations of the pulsating flow of cerebrospinal fluid flow in the cervical spinal canal of a chiari patient, *J. Biomech.* 47 (2014) 1082–1090.
- [8] H. Ahmad, S.Y. Jung, Effect of active and passive cooling on the thermo-hydrodynamic behaviors of the closed-loop pulsating heat pipes, *Int. J. Heat Mass Transf.* 156 (2020) 119814.
- [9] M.A. Nazari, M.H. Ahmadi, R. Ghasempour, M.B. Shafii, O. Mahian, S. Kalogirou, S. Wongwises, A review on pulsating heat pipes: from solar to cryogenic applications, *Appl. Energ.* 222 (2018) 475–484.
- [10] I. Levitsky, D. Tavor, V. Gitis, Microbubbles, oscillating flow, and mass transfer coefficients in air-water bubble columns, *J. Water Process Eng.* 49 (2022) 103087.
- [11] Y. Cui, C. Li, W. Zhang, X. Ning, X. Shi, J. Gao, X. Lan, A deep learning-based image processing method for bubble detection, segmentation, and shape reconstruction in high gas holdup sub-millimeter bubbly flows, *Chem. Eng. J.* 449 (2022) 137859.
- [12] V. Papadopoulou, S. Evgenidis, R.J. Eckersley, T. Mesimeris, C. Balestra, M. Kostoglou, T. Karapantsios, M.X. Tang, Decompression induced bubble dynamics on ex vivo fat and muscle tissue surfaces with a new experimental set up, *Colloids Surf. b: Biointerfaces* 129 (2015) 121–129.
- [13] V.P. Nikolayev, Simulation of gas bubble growth and dissolution in human tissues during dives and recompression, *Aviat. Space Environ. Med.* 84 (2013) 938–945.
- [14] J. Zueco, A. Hernández-González, Electric analogue for the dynamics of decompression sickness bubbles: numerical results, *Acta Astronaut.* 66 (2010) 59–69.

- [15] J. Zueco, L.M. Lopez-Gonzalez, Network model to study physiological processes of hypobaric decompression sickness: new numerical results, *Acta Astronaut.* 121 (2016) 256–270.
- [16] R. Arieli, A. Marmur, Evolution of bubbles from gas micronuclei formed on the luminal aspect of ovine large blood vessels, *Respir. Physiol. Neurobiol.* 188 (2013) 49–55.
- [17] R. Arieli, A. Marmur, Ex vivo bubble production from ovine large blood vessels: size on detachment and evidence of active spots, *Respir. Physiol. Neurobiol.* 200 (2014) 110–117.
- [18] R. Arieli, U. Arieli, A. Marmur, Bubble size on detachment from the luminal aspect of ovine large blood vessels after decompression: the effect of mechanical disturbance, *Respir. Physiol. Neurobiol.* 216 (2015) 1–8.
- [19] J.E. Blatteau, H.N. David, N. Vallee, C. Meckler, S. Demaistre, J.J. Risso, J. E. Abraini, Cost-efficient method and device for the study of stationary tissular gas bubble formation in the mechanisms of decompression sickness, *J. Neurosci. Methods* 236 (2014) 40–43.
- [20] R. Arieli, A. Marmur, Expansion of bubbles under a pulsatile flow regime in decompressed ovine blood vessel, *Respir. Physiol. Neurobiol.* 222 (2016) 1–5.
- [21] R. Arieli, In vitro evidence of decompression bubble dynamics and gas exchange on the luminal aspect of blood vessels: implications for size distribution of venous bubbles, *Physiol. Rep.* 7 (2019) 14317.
- [22] S.P. Evgenidis, T. Karapantsios, Effect of bubble size on void fraction fluctuations in dispersed bubble flows, *Int. J. Multiph. Flow.* 75 (2015) 163–173.
- [23] S.P. Evgenidis, T. Karapantsios, Gas–liquid flow of sub-millimeter bubbles at low void fractions: experimental study of bubble size distribution and void fraction, *Int. J. Heat Fluid Fl.* 71 (2018) 353–365.
- [24] P. Gkotsis, S.P. Evgenidis, T. Karapantsios, Influence of newtonian and non-newtonian fluid behaviour on void fraction and bubble size for a gas-liquid flow of sub-millimeter bubbles at low void fractions, *Exp. Therm. Fluid. Sci.* 109 (2019) 109912.
- [25] P. Gkotsis, S. Evgenidis, T.D. Karapantsios, Associating void fraction signals with bubble clusters features in co-current, upward gas-liquid flow of a non-newtonian liquid, *Int. J. Multiph. Flow.* 131 (2020) 103297.
- [26] S.P. Evgenidis, T.D. Karapantsios, Gas–liquid flow of sub-millimeter bubbles at low void fractions: void fraction prediction using drift-flux model, *Exp. Therm. Fluid. Sci.* 98 (2018) 195–205.
- [27] S.P. Evgenidis, T.D. Karapantsios, Pulsatile gas-liquids flow resembling decompression sickness: computational fluid dynamics simulation and experimental validation, *Int. Marit. Health* 73 (4) (2022) 189–198.
- [28] S.P. Evgenidis, T.D. Karapantsios, 3D simulation of pulsatile bubbly flow resembling decompression sickness conditions inside a realistic human artery, *Exp. Comput. Multiph. Flow* 6 (2) (2024) 135–139.
- [29] R.D. Vann, F.K. Butler, S.J. Mitchell, R.E. Moon, Decompression illness, *The Lancet* 377 (2011) 153–164.
- [30] S.P. Evgenidis, A. Chondrou, T. Karapantsios, A new phantom that simulates electrically a human blood vessel surrounded by tissues: development and validation against in-vivo measurements, *Ann. Biomed. Eng.* 6 (2023) 1284–1295.
- [31] O. Oikonomidou, S.P. Evgenidis, M. Kostoglou, T.D. Karapantsios, Degassing of a pressurized liquid saturated with dissolved gas when injected to a low pressure liquid pool, *Exp. Therm. Fluid. Sci.* 96 (2018) 347–357.
- [32] O. Oikonomidou, S.P. Evgenidis, C.J. Schwarz, J.J.W.A. van Loon, M. Kostoglou, T. D. Karapantsios, Degassing of a decompressed flowing liquid under hypergravity conditions int, *J. Multiph. Flow* 115 (2019) 126–136.
- [33] W. Tzevelekos, Q. Galand, S. Evgenidis, K. Zacharias, T. Karapantsios, S. Vaerenbergh, High-resolution concentration measurement in water/n-butanol binary system by means of high-frequency electrical impedance method, *Exp. Therm. Fluid. Sci.* 126 (2021) 110399.
- [34] S.P. Evgenidis, K. Zacharias, V. Papadopoulou, S. Theunissen, C. Balestra, T. D. Karapantsios, In-field use of I-VED electrical impedance sensor for assessing post-dive decompression stress in humans, *Undersea Hyperbar. m.* 51 (1) (2024) 71–83.
- [35] R.H.S. Winterton, J.S. Munaweera, Bubble size in two-phase gas–liquid bubbly flow in ducts, *Chem. Eng. Process.* 40 (2001) 437–447.
- [36] J.C. Maxwell, A treatise of electricity and magnetism, Oxford University Press, London, 1892.
- [37] X. Zabulis, M. Papara, A. Chatziargyriou, T.D. Karapantsios, Detection of densely dispersed spherical bubbles in digital images based on a template matching technique: application to wet foams, *Colloids Surf. a: Physicochem. Eng. Aspects* 309 (2007) 96–106.
- [38] W.D. Deckwer, Bubble column reactors, John Wiley and Sons, England, 1992.
- [39] S.P. Evgenidis, N.A. Kazakis, T.D. Karapantsios, Bubbly flow characteristics during decompression sickness: effect of surfactant and electrolyte on bubble size distribution, *Colloids Surf. a: Physicochem. Eng. Aspects* 365 (2010) 46–51.
- [40] S. Majumder, G. Kundu, D. Mukherjee, Bubble size distribution and gas–liquid interfacial area in a modified downflow bubble column, *Chem. Eng. J.* 122 (2006) 1–10.
- [41] J.P. Woodcock, Physical properties of blood and their influence on blood-flow measurement, *Rep. Prog. Phys.* 39 (1975) 65–127.
- [42] M.Y. Yousif, D.W. Hodsworth, T.L. Poepping, A blood-mimicking fluid for particle image velocimetry with silicone vascular models, *Exp. Fluids* 50 (2011) 769–774.
- [43] Z. Taitel, D. Bornea, A.E. Dukler, Modeling flow pattern transitions for steady upward gas-liquid flow in vertical tubes, *A. i. Ch. e. J.* 26 (1980) 345–354.
- [44] A.D. Passos, V.P. Voulgaropoulos, S.V. Paras, A.A. Mouza, The effect of surfactant addition on the performance of a bubble column containing a non-newtonian liquid, *Chem. Eng. Res. Des.* 95 (2015) 93–104.
- [45] Q. Xu, M. Nakajima, S. Ichikawa, N. Nakamura, P. Roy, H. Okadome, T. Shiina, Effects of surfactant and electrolyte concentrations on bubble formation and stabilization, *J. Colloid Interface Sci.* 332 (2009) 208–214.
- [46] A. Riquelme, A. Desbiens, R. del Villar, M. Maldonado, Identification of a nonlinear dynamic model of the bubble size distribution in a pilot flotation column, *Int. J. Miner. Process.* 145 (2015) 7–16.
- [47] S.S. Alves, S.P. Orvalho, J.M.T. Vasconcelos, Effect of bubble contamination on rise velocity and mass transfer, *Chem. Eng. Sci.* 60 (2005) 1–9.